Supporting Information

Sun et al. 10.1073/pnas.1418075111

SI Text

Development of a Global Mesophyll Conductance (g_m) Model. A model of mesophyll conductance (g_m) suitable for global applications has not previously been available. We develop such an empirical g_m model by synthesizing the latest advances in field plant physiological studies. Large-scale carbon cycle models generally use the concept of plant functional types (PFTs) to simulate carbon, water, and energy fluxes of terrestrial ecosystems. We use a similar strategy to develop a global g_m model so that it is consistent with large-scale modeling philosophy and applicable broadly to different vegetation types, rather than to particular ecosystems. Field measurements have shown that g_m varies with leaf structures and environmental conditions (1–4). Leaf structures determine the maximum attainable g_m with external environmental forcings modifying this maximum value. This consensus reflects a recent understanding that environmental stress factors (e.g., temperature and water) can induce rapid physiological changes (e.g., hardening of cell walls and aquaporin-mediated alteration of membrane permeability) that cause g_m to vary on time scales of minutes to hours (5–8). Accordingly, we model g_m as

$$g_m = g_{\max 0} \cdot f_l(x) \cdot f_T(T_l) \cdot f_w(\theta), \quad \textbf{[S1]}$$

where $g_{\max 0}$ is the maximum g_m (i.e., a value of g_m under nonstress conditions, here referring to the presence of ample soil water and a temperature of 25 °C) of a leaf at the canopy top of a PFT; $f_l(x)$ represents the vertical variation of g_m as a function of cumulative leaf area index x from canopy top, driven by light gradient within the canopy; and $f_T(T_l)$ and $f_w(\theta)$ are the response functions of g_m to leaf temperature T_l and to soil moisture θ, respectively.

The present study makes no attempt to represent other potential environmental effects, e.g., salinity, O_3, nutrient availability (4), on g_m because these effects are much less well understood and seldom quantified in field studies. Also we do not consider the potential rapid, direct responses of g_m to changes in ambient CO_2 concentration and irradiance reported in some previous studies as a recent analysis shows that such responses may be due to methodological artifacts in experiments (9). There is also the possibility that the spatial separation between Rubisco and the releasing site of CO_2 from dark respiration and photorespiration (mitochondria) may render g_m to be a composite variable, rather than a stable parameter (10). This possibility can be addressed with a two-component model of mesophyll conductance (10). However, currently there are no data available to parameterize this two-component model. Fortunately, observations often show that in C_3 plant species, mitochondria occupy the center of the cell and are surrounded by chloroplasts that are positioned just under the plasmalemma (11). In such a spatial configuration, CO_2 molecules evolved from mitochondria and released into cytosol must first diffuse through chloroplasts to reach the intercellular air space. From a modeling point of view, this arrangement has the same effect as if Rubisco and mitochondria shared the same compartment (12). Sun et al. (13) and Gu and Sun (9) used simulations to demonstrate that a single g_m model is sufficient for the purpose of modeling photosynthesis. Therefore, in this study, we adopt the framework of a single g_m model.

The $g_{\max 0}$ varies significantly across plant species. A synthesis of measurements for ∼100 plant species showed that this term is related to the leaf dry mass per unit area M_a through an empirical power law (2)

$$g_{\max 0} = a \cdot M_{a0}^{b}, \quad \textbf{[S2]}$$

where M_{a0} represents M_a at canopy top. The constants a = 24.240338 and b = −0.6509 are two empirical parameters that have been determined by fitting compiled data to Eq. **S2** [r^2 = 0.79; $P < 0.001$; see figure 2.1 in Niinemets et al. (2)]. All empirical constants used in our global mesophyll conductance model are listed in Table S1. Similar patterns were also reported in other studies (4, 14) but with fewer species samples. The values of a and b depend on the units of data used for the nonlinear regression of Eq. **S2**. Our study uses μmol/m^2/s/Pa for $g_{\max 0}$ and g_m, and g/m^2 for M_{a0} and M_a. The coefficient b is negative, indicating $g_{\max 0}$ decreases with M_{a0} across PFTs under nonstress conditions. The $g_{\max 0}$ in Eq. **S2** is area based, whereas Niinemets et al. (2) used a mass-based unit. The area- and mass-based $g_{\max 0}$ differ by a factor of M_{a0}. Accordingly, the value of b in our study is a notation on an area basis. In Eq. **S2**, $g_{\max 0}$ is represented as a leaf trait associated with PFTs because it is determined by M_{a0}, which is the product of two important leaf traits: leaf thickness and foliar mass density (2).

Multiple steps are needed to derive an expression for $f_l(x)$, which describes the variation of g_m associated with the prevailing light regime within a plant canopy. The light intensity shapes the mesophyll cell morphology, the number of mesophyll cell layers, and the leaf thickness. These factors are components that determine $M_a(x)$, the leaf dry mass per area at a cumulative leaf area index x (15). They also affect the total surface area of mesophyll cells exposed to intercellular air space per unit leaf area and hence g_m (2, 11). Consequently, g_m tends to change systematically from top to bottom of a canopy (16–22) and scales well with the variation of $M_a(x)$ with canopy depth (18, 21). Therefore, $M_a(x)$ is an important link between g_m and the prevailing light gradient within a canopy. Here this vertical variation of g_m is modeled as follows:

$$g_{\max}(x) = g_{\max 0} \cdot [M_a(x)/M_{a0}]^{d}, \quad \textbf{[S3]}$$

where d = 0.8109, an empirical parameter fitted from the data (r^2 = 0.67) in Montpied et al. (21). Rearranging Eq. **S3**, we have

$$f_l(x) = g_{\max}(x)/g_{\max 0} = [M_a(x)/M_{a0}]^{d}. \quad \textbf{[S4]}$$

According to Niinemets (15), $M_a(x)$ is related to the seasonally integrated photosynthetic active radiation $I(x)$ via

$$M_a(x) = M_{a0} \cdot [I(x)/I_0]^{f}, \quad \textbf{[S5]}$$

where I_0 is the value of $I(x)$ at canopy top; f = 0.221897, a parameter fitted (r^2 = 0.57) from Niinemets (15). Applying the Beer's law

$$I(x) = I_0 \cdot \exp(-k_I \cdot x), \quad \textbf{[S6]}$$

where k_I = 0.50, a commonly used value for the seasonally averaged light extinction coefficient (23, 24), and substituting Eqs. **S6** and **S5** to Eq. **S4**, we obtain

$$f_l(x) = \exp(-k_I \cdot d \cdot f \cdot x) = \exp(-k_g \cdot x). \quad \textbf{[S7]}$$

Here, $k_g = k_I \cdot d \cdot f$ = 0.08997, a composite parameter that is the product of three empirical coefficients k_I, d, and f. Eq. **S7** shows

that the vertical variation of g_m within a canopy can be modeled as an exponentially decreasing function of cumulative leaf area index x from the top of canopy, characterized with a single decay coefficient k_g. The advantage of creating a single composite parameter k_g is that it facilitates the sensitivity test with this parameter, which may guide process-based measurements. The joint control of M_{a0} and x on g_m is illustrated in Fig. S1, showing that g_m decreases with M_{a0} and x.

It is important to clarify that the dependence of $g_{\max 0}$ on M_{a0} in Eq. **S2** is fundamentally different from the relationship between g_m and $M_a(x)$ in Eq. **S3**. Eq. **S2** applies across PFTs, whereas Eq. **S3** is used to formulate $f_I(x)$ and applies to the depth of a canopy within a PFT. $M_a(x)$ is a composite leaf structural variable and is modified by the prevailing vertical gradient in light regime within a plant canopy. The variations of leaf structures along canopy depth and thus $M_a(x)$ are different from the variations of leaf structures across leaf forms of PFTs and thus the composite leaf trait M_{a0}. As stated earlier, the light intensity gradient along the canopy depth affects $M_a(x)$ through its effects on the mesophyll cell morphology, the number of mesophyll cell layers, and the leaf thickness. In contrast, the variations of M_{a0} across leaf forms of PFTs reflect the changes in leaf robustness, e.g., the compactness of mesophyll cells, the thickness of cell walls, and the foliar mass density. Detailed discussion on this issue is beyond the scope of this paper but can be found elsewhere (2, 11).

Several functions have been proposed to describe the temperature response of g_m (5, 25–27). Here the formulation of Bernacchi et al. (5), which was based on detailed measurements and showed agreement with data from independent researchers (28), is used

$$f_T(T_l) = \exp[c - \Delta H_a/(R \cdot T_l)]/\{1 + \exp[(\Delta S \cdot T_l - \Delta H_d)/(R \cdot T_l)]\}, \quad \textbf{[S8]}$$

where $c = 20.0$, a scaling constant; $\Delta H_a = 49.6 \times 10^3$ J/mol, the activation energy; $\Delta H_d = 437.4 \times 10^3$ J/mol, the deactivation energy; $\Delta S = 1.4 \times 10^3$ J/mol/K, an entropy term; and $R = 8.314$ J/mol/K, the universal gas constant. Eq. **S8** is normalized to 25 °C; hence, $f_T(25\ ^\circ\text{C}) = 1$. It features an initial increase of g_m with T_l (10–35 °C) and decline at high T_l, thus allowing simulation of high temperature inhibition.

Different forms of the water stress term have been applied to g_m in canopy models (29–32). For convenience, we use the CLM4.5 water stress function (33), which has already been applied to V_{cmax} and stomatal conductance g_s (34). In the CLM4.5 formulation

$$f_w(\theta) = \sum_i^n f_{\text{root},i} \cdot w_i(\theta), \quad \textbf{[S9]}$$

where n is the total number of soil layers; $f_{\text{root},i}$ is the root fraction within soil layer i; and $w_i(\theta)$ is the plant wilting factor, derived from the soil water content θ for each layer. The calculation of $f_{\text{root},i}$ and $w_i(\theta)$ follows CLM4.5 procedures (33). The term $f_w(\theta)$ ranges from 1 (wet soil) to ~0 (dry soil), depending on the soil water potential of each layer, and root distribution of PFTs.

Implementation of a Global g_m Model in CLM4.5. CLM4.5 divides the canopy into sunlit and shaded fractions and calculates photosynthesis separately for these two groups of leaves. To be consistent with the CLM4.5 canopy integration scheme, the mean, weighted g_m for sunlit and shaded fractions is calculated, respectively, as

$$\overline{g_{\max\_sun}} = g_{\max 0} \frac{\int_0^L \exp(-k_g \cdot x) \cdot f_{sun}(x) dx}{\int_0^L f_{sun}(x) dx} = g_{\max 0} \cdot \frac{k_b}{k_g + k_b} \cdot \frac{1 - \exp[-(k_g + k_b) \cdot L]}{1 - \exp(-k_b \cdot L)}, \quad \textbf{[S10a]}$$

$$\overline{g_{\max\_sha}} = g_{\max 0} \frac{\int_0^L \exp(-k_g \cdot x) \cdot [1 - f_{sun}(x)] dx}{\int_0^L [1 - f_{sun}(x)] dx} = g_{\max 0} \cdot \frac{k_b}{k_g (k_g + k_b)} \cdot \frac{k_b - (k_g + k_b) \cdot \exp(-k_g \cdot L) + k_g \cdot \exp[-(k_g + k_b) \cdot L]}{\exp(-k_b \cdot L) - 1 + k_b \cdot L}. \quad \textbf{[S10b]}$$

Here, L is the leaf area index; and k_b is the direct beam extinction coefficient and is used to calculate $f_{sun}(x)$ and $f_{sha}(x)$, the fractions of sunlit and shaded leaves respectively. k_I in Eqs. **S6** and **S7** differs from k_b in that k_I is a seasonal mean, whereas k_b varies with solar zenith angle and thus the course of a day and throughout a year and hence is typically updated each time step in model simulations.

g_m links the CO_2 concentration inside leaf chloroplast (C_c) and that at intercellular air space (C_i) with the net carbon assimilation rate A through $C_c = C_i - A/g_m$. Here C_c and C_i are in units of Pa because A and g_m are in units of μmol/m^2/s and μmol/m^2/s/Pa, respectively; elsewhere in the paper, CO_2 concentrations are expressed in units of ppm. The original CLM4.5 used a numerical scheme to solve for photosynthesis by iterating over C_i. In the g_m-enabled CLM4.5, we iterate over C_c and A is calculated with the photosynthesis model from C_c.

$g_{\max 0}$ is obtained from M_{a0}, which in turn is calculated from the inverse of the canopy-top specific leaf area SLA_0 [m^2(gC)], a parameter already specified in CLM4.5 (Fig. S1). M_{a0} (g/m^2) in Eq. **S2** differs from $1/SLA_0$ (gC/m^2) by a factor of two because the former refers to total leaf dry mass, whereas the latter includes only the carbon fraction. Our g_m model is applicable only to C_3 plants; the calculations for C_4 photosynthesis are unchanged in the present study.

Conversion of the g_m-Lacking to g_m-Including Photosynthetic Parameters for CLM4.5. The development and implementation of a global g_m model allows photosynthesis to be calculated at the correct CO_2 concentration; that is, the CO_2 concentration at the site of carboxylation inside the chloroplast. Accordingly, the fundamental biochemical photosynthetic parameters (i.e., V_{cmax}, $J_{\max}$, and TPU) of the FvCB model used in conjunction with the g_m model must reflect the actual photosynthetic capacities of the chloroplast. Current global carbon cycle models use phenomenological photosynthetic parameters (i.e., the g_m-lacking parameters) that are smaller than the true photosynthetic capacities (i.e., the g_m-including parameters) of the chloroplast because their derivation did not represent mesophyll diffusion of CO_2 explicitly (13, 35–37). A matching correspondence between the g_m-including and g_m-lacking photosynthetic parameters must be established so that the dynamic behaviors of carbon cycle models with and without explicit representation of mesophyll diffusion can be compared.

A complication in establishing the matching correspondence between the g_m-including and g_m-lacking fundamental photosynthetic parameters is that at least two different forms of the FvCB model have been used to model leaf photosynthesis. There

is no a priori argument that the correspondence between the g_m-including and g_m-lacking parameters is invariant between the different forms of the FvCB model. In one form, which we call the monolimiting form [see, for example, the implementation in Gu et al. (38)], the net photosynthetic rate A is given by the following expression:

$$A = \min\{W_c, W_j, W_p\}(1-\Gamma^*/C_c) - R_d, \qquad \textbf{[S11]}$$

where W_c, W_j, and W_p represent the carbon carboxylation rate limited by Rubisco, RuBp regeneration, and TPU, respectively, and Γ^* and R_d denote the chloroplastic CO_2 photosynthetic compensation point and day respiration, respectively. In the monolimiting FvCB model, the smallest of three limitations exclusively defines the photosynthetic rate for any particular set of forcing conditions, whereas the other two limitations play no role (except that they help to determine which one is the smallest). It is the most frequently used form. In another form, which is called the colimiting form (39), A is given by the smaller root of the following equations:

$$\begin{aligned} &\Theta_{cj}A_i^2 - (A_c + A_j)A_i + A_cA_j = 0 \\ &\Theta_{ip}(A+R_d)^2 - (A_i + A_p)(A+R_d) + A_iA_p = 0, \end{aligned} \qquad \textbf{[S12]}$$

where A_i in the first equation is a transient variable for calculating A in the second equation; Θ_{cj} and Θ_{ip} are two fixed empirical curvature parameters (0.98 and 0.95, respectively, in CLM4.5); and A_c, A_j, and A_p are, respectively, given by

$$\begin{aligned} A_c &= W_c(1-\Gamma^*/C_c) \\ A_j &= W_j(1-\Gamma^*/C_c) \\ A_p &= W_p(1-\Gamma^*/C_c). \end{aligned} \qquad \textbf{[S13]}$$

In contrast to the monolimiting FvCB model, the colimiting FvCB model calculates the photosynthetic rate for any particular set of forcing conditions with inputs from all three limitations, although its value is dominated by the most limiting of the three limitations (when Θ_{cj} and Θ_{ip} are set to 1, the mono- and colimiting FvCB models are identical).

Sun et al. (13) showed that, for the monolimiting FvCB model, the following relationship can be used to estimate the g_m-including parameters accurately from the corresponding g_m-lacking parameters if g_m is known:

$$y = w\exp\left(p\frac{w^u}{g_m^q + v}\right). \qquad \textbf{[S14]}$$

Here (w, y) represents the pairs of g_m-lacking and g_m-including V_{cmax}, J_{max}, and TPU at a reference temperature of 25 °C; and p, q, u, and v are empirical constants and differ among these pairs (Table S2). To estimate p, q, u, and v in Eq. **S14**, Sun et al. (13) used a worldwide database of leaf gas exchange measurements collected by LeafWeb (leafweb.ornl.gov). The measurements used in Sun et al. (13) contained more than 1,000 A/C_i curves from nearly 130 C_3 plant species covering all major plant functional types of the world, which include grasses, herbs, crops, shrubs, and trees (deciduous and evergreen broadleaf and conifers). These curves were analyzed for g_m-lacking and g_m-including V_{cmax}, J_{max}, and TPU, as well as g_m with an optimization approach (36, 38). The obtained parameters are then used to estimate the empirical constants in Eq. **S14**.

However, CLM4.5 in contrast to its earlier versions applies the colimiting FvCB model and also somewhat different temperature response functions (33, 34). To ensure consistency and comparability between the g_m-lacking and g_m-including simulations, we reanalyzed the LeafWeb A/C_i curves for g_m-lacking and g_m-including V_{cmax}, J_{max}, and TPU, as well as g_m with exactly the same formulations of the FvCB model and temperature response functions used by CLM4.5. The obtained parameters are then used to reestimate p, q, u, and v in Eq. **S14**. The reestimated p, q, u, and v are given in Table S2. For convenience, we use monolimiting and colimiting conversion functions to denote Eq. **S14** with the empirical constants estimated for the monolimiting and colimiting FvCB models, respectively.

Fig. S2 shows the relationship between the g_m-including parameters estimated directly from the A/C_i curves for the colimiting FvCB model and those calculated from the colimiting conversion function. The agreement is reasonable for V_{cmax}, J_{max}, and TPU, although the monolimiting conversion function appears to fit better overall [compare Fig. S2 with figure 5 in Sun et al. (13)]. Fig. S3 compares the difference between the mono- and colimiting conversion functions for a few selected values of g_m. Both conversion functions show that V_{cmax} is the most sensitive, TPU is the least sensitive, and J_{max} has an intermediate sensitivity to g_m. However, the colimiting V_{cmax} and J_{max} appear to be more sensitive to g_m than their monolimiting counterparts, whereas the opposite is true for TPU. In fact, the colimiting TPU differs little between with and without explicit consideration of mesophyll diffusion such that all empirical constants are effectively zero for the colimiting TPU conversion function (Table S2).

Because the empirical constants in the colimiting conversion function are estimated in accordance with CLM4.5 photosynthetic model formulations, we report global simulation results based on the colimiting conversion function. However, the colimiting conversion function may be more uncertain than the monolimiting conversion function as the fitting of an A/C_i curve with the colimiting FvCB model is considerably more difficult than with the monolimiting FvCB model. In any A/C_i curve measurement, one or two carboxylation limitation states (Rubisco, RuBP regeneration, and TPU) may be missing (40, 41). When the monolimiting FvCB model is used to fit the data, any missing limitation state can be detected and its associated parameters be removed from the parameter estimation process with the enumeration strategy developed by Gu et al. (38). In contrast, the application of the colimiting FvCB model has to simply assume all three limitation states are always present in the data, which may or may not be true for any particular curve. Consequently, more unreasonable parameter values are produced with the colimiting FvCB model and have to be disqualified according to the objective criteria proposed in Gu et al. (38). Even after the application of this data quality control procedure, there are still some unusually large parameter values compared with those obtained for the monolimiting FvCB model [compare Fig. S2 with figure 5 in Sun et al. (13); the same original dataset are used in both analyses], indicating not all curves used in the final fitting contain sufficient constraining power for parameter estimation for the colimiting conversion function. As a precaution, the monolimiting conversion function is also applied in additional global simulations so that impacts of uncertainty in the conversion function can be evaluated.

CLM4.5 accounts for the influence of day length $f(D)$ on (g_m-lacking) V_{cmax} (adjusted to 25 °C), i.e., $V_{cmax} = V^0_{cmax}\cdot f(D)$. Here V^0_{cmax} is the value of V_{cmax} unattenuated by shortening in day length. The same $f(D)$ is propagated to J_{max} and TPU (at 25 °C) via their linear dependence on V_{cmax}. We perform parameter conversion on the unattenuated (g_m-lacking) parameters (PFT-specific) and then apply the factor $f(D)$ to the corresponding, converted g_m-including values. In this way, we preserve the functional relationships among the fundamental photosynthetic parameters both before and after the conversion (13). Finally, the conversions of photosynthetic parameters are all performed on values at canopy top so that the vertical profiles of photosynthetic parameters are not altered. In short, the canopy integration strategy of the g_m-enabled CLM4.5 is not altered from

that of the original CLM4.5, which helps ensure that any difference between the g_m-lacking and g_m-including simulations is caused entirely by the explicit consideration of mesophyll diffusion. Table S3 compares g_m-lacking and g_m-including photosynthetic parameters in CLM4.5 with either monolimiting or colimiting conversion functions.

Global Simulations and Consistency Checks. Because mesophyll diffusion of CO_2 affects gross primary production (GPP) directly and because GPP is the first step of the terrestrial carbon cycle, we focus on GPP in this current study. The cascade effects of mesophyll diffusion through GPP on downstream carbon processes are also important to recognize. However, models of terrestrial carbon cycling are complicated and many processes are represented without precise knowledge. As the first study (to our knowledge) of mesophyll diffusion effects at the global scale, focusing on GPP provides a clear demonstration of the impact of mesophyll diffusion and a direct explanation of the cause of its impact.

We also decided to conduct simulations only on a historical period (1901–2010) for which observational forcing data are available. Thus, our estimation of impact of mesophyll diffusion is likely to be conservative because this impact is expected to be more important on long term than on short term and for the historical period, models, including the g_m-lacking models, are presumably already well calibrated. An extension of the simulations to future climate, for example, to 2100 using representative concentration pathways (RCPs) of the Intergovernmental Panel on Climate Change (IPCC) should show larger impacts of mesophyll diffusion. However, focusing on a relatively short historical period removes many uncertainties inherently involved in making future prediction and allows us to concentrate on illuminating processes and mechanisms rather than on showing magnitudes.

As stated earlier, for the objective of this study, it is important to ensure that any difference between the g_m-lacking and g_m-including simulations is caused entirely by an explicit consideration of mesophyll diffusion. That is why strict correspondence between g_m-lacking and g_m-including fundamental photosynthetic parameters must be established. However, ensuring this strict parameter correspondence is not sufficient to obtain comparable simulations. We must also make sure that the g_m-lacking and g_m-including simulations are done for the same model terrestrial biosphere. This is achieved by using the same state variables (e.g., CLM4.5 specified leaf area indices) in all our simulations. This strategy also avoids potentially large biases in prognostically evolving state variables of the biosphere which can be caused by, for example, uncertainties in the representations of limitations of nutrients (particularly nitrogen and phosphorous) on photosynthesis.

Multiple simulations are carried out to clarify and quantify the dynamic behaviors of CLM4.5 with or without the developed g_m model implemented (Table S4): the CTRL run, a control simulation with the original CLM4.5 that has no explicit representation of mesophyll diffusion; the IMED run, a simulation that incorporates the developed g_m model only but retains the original g_m-lacking photosynthetic parameters in CLM4.5; and the MESO run, a simulation with both the explicit consideration of mesophyll diffusion and the corresponding g_m-including photosynthetic parameters. The MESO run is repeated with the colimiting and monolimiting conversion functions as a test for the effect of uncertainty in the conversion function. The IMED run serves as an intermediate step to illustrate the effect of incorporating a g_m model and also as a consistency check. Because the g_m-lacking photosynthetic parameters are smaller than the corresponding g_m-including photosynthetic parameters (13, 35–37) and because the implementation of a g_m model will lead to reduced CO_2 concentrations at the site of carboxylation, we expect the annual GPP of the IMED run will be smaller than either that of the CTRL run or that of the MESO run if the g_m model and the conversion function have been applied correctly in CLM4.5. We also carry out two additional experiments to provide baseline references for quantifying the historical CO_2 fertilization effect on GPP: CTRL_cCO_2 and MESO_cCO_2, both of which are similar to CTRL and MESO except that the atmospheric CO_2 concentration is fixed at the level of year 1901, i.e., 296 ppm.

All simulations are offline experiments driven by the CRU/NCEP/NCAR reanalysis (www.cru.uea.ac.uk/cru/data/ncep/). The historical atmospheric CO_2 concentrations, which are used in all simulations except in constant CO_2 runs, are derived from ice cores and atmospheric observations (42). All simulations have a spatial resolution of 1.9° × 2.5° with a prescribed transient land cover (33, 43).

We compare the mean global annual GPP of 1985–2004 from different runs with the reanalysis climate and observed atmospheric CO_2 concentrations to ensure that the g_m-enabled CLM4.5 behaves as expected. From 1985 to 2004, the atmospheric CO_2 concentration increased from 345 to 377 ppm. The CTRL run estimates the global annual GPP to be 145.17 PgC/y averaged over the period of 1985–2004 (Fig. S4*A*). The IMED run reduces the mean global annual GPP by ∼15 PgC/y (Fig. S4 *B* and *D*) compared with CTRL. This reduction is consistent with our expectation as mentioned above. The GPP decrease is throughout the globe, but most prevalent in the tropics. The use of a g_m model together with the g_m-including photosynthetic parameters in the MESO run with the colimiting conversion function leads to a mean annual GPP of 146.60 PgC/y, a slight increase of ∼1 PgC/y compared with CTRL (Fig. S4*C*) and about 17 PgC/y higher than the IMED run, again consistent with expectation. The mean annual GPP for the MESO run with the monoconversion function is 144.60 PgC/y, a less than 1 PgC/y decrease from CTRL and more than 15 PgC/y higher than IMED, again consistent with expectations.

Currently there are no direct global GPP measurements to verify our simulation results. Published estimates of contemporary global GPP are highly uncertain. One estimate based on scaled-up eddy flux measurements coupled with diagnostic models placed global GPP at 123 PgC/y (44). A different approach using atmospheric oxygen isotopes suggested 150–175 PgC/y (45). Thus, our simulated GPP values for the MESO runs for the contemporary time (1985–2004) are in the middle of these published estimates.

The comparisons among the CTRL, IMED, and MESO runs indicate that our implementation of the global g_m model in CLM4.5 is internally consistent. This internal consistency is an important check on representation of mesophyll diffusion in CLM4.5 because our g_m model and the parameter conversion function are independently derived. These comparisons also demonstrate that it is important to update the g_m-lacking photosynthetic parameters to the corresponding g_m-including photosynthetic parameters in models that represent mesophyll diffusion explicitly; without doing so, the models would not be self-consistent.

Fig. S5 shows the difference in the CO_2 fertilization effect (ΔCFE) on GPP between the g_m-including and g_m-lacking CLM4.5 when the monolimiting conversion function is used in the simulations. The results are similar to those with the colimiting conversion function (compare Fig. S5 with Fig. 1), even though the two conversion functions differ somewhat (Fig. S3). This similarity suggests that any imperfection in establishing the matching correspondence between the g_m-including and g_m-lacking biochemical parameters through the parameter conversion functions does not fundamentally alter our findings.

Under What Conditions Do the g_m-Lacking and g_m-Including Models Match? Comparison of absolute values of GPP predicted by g_m-lacking and g_m-including models is not an appropriate way of

evaluating the impact of explicit representation of mesophyll diffusion on modeling the long-term trend of the CO_2 fertilization effect because the two models may have different baseline references against which the fertilization effects are quantified. However, a direct comparison of absolute values of GPP can help identify conditions under which the phenomenological photosynthetic parameters can be used to compensate for the effect of the model structural deficiency due to a lack of explicit representation of mesophyll diffusion. Fig. S6 shows the temporal variation of the difference in the annual global GPP simulated with CLM4.5 between with and without explicit consideration of mesophyll diffusion. Before the early1970s (atmospheric $CO_2 < 320$ ppm), the g_m-lacking model predicts a higher GPP, and after the middle 1980s (atmospheric $CO_2 > 350$ ppm), it predicts a lower GPP compared with the g_m-including model. From the early 1970s to the middle 1980s (320–350 ppm), the two models have similar GPP. Thus, 320–350 ppm is the range of ambient CO_2 for which the g_m-lacking model is adequate for simulating GPP.

The minimal bias of the g_m-lacking model for a range of ambient CO_2 in some intermediate past probably reflects the history of model development and calibration. It is interesting to note that 320–350 ppm is generally within the range of ambient CO_2 emphasized in leaf gas exchange measurements and thus is well constrained in curve fitting for photosynthetic parameters (40, 41). Therefore, Fig. S6 may be viewed as a vindication of a well-known modeling principle: a structurally deficient model may work well for the conditions to which its parameters are carefully tuned, but once the conditions deviate from the tuning conditions, its reliability becomes questionable. This general principle evidently applies to carbon cycle models.

Analyses of Leaf-Scale CO_2 Fertilization Effect Based on Leaf Gas Exchange Measurements

Leaf gas exchange measurements (A/C_i curves) collected by LeafWeb (leafweb.ornl.gov) were used in this study for two purposes. One was to determine the empirical constants in the conversion function (Eq. **S14**). The other was to analyze the difference in leaf-scale CO_2 fertilization effect between models with and without explicit consideration of mesophyll diffusion. Both tasks depended on the paired g_m-including and g_m-lacking V_{cmax}, J_{max}, and TPU, as well as g_m estimated from these A/C_i curves (13, 38).

The leaf-scale analyses (Fig. 4) used directly in the calculations more than 1,000 pairs of g_m-including and g_m-lacking photosynthetic parameters and g_m values, removing any uncertainty that may be related to the parameter conversion function or to the global g_m model. The leaf-scale simulations are run at multiple levels of PPFD and temperature and also at all measurement conditions of the original A/C_i curves from which the g_m-including and g_m-lacking photosynthetic parameters and g_m are estimated. The average measurement conditions of the original A/C_i curves are $1{,}255 \pm 323$ μmol/m^2/s for PAR and 26 ± 5 °C for temperature. From these leaf-scale runs, the ratio R of the g_m-including to g_m-lacking β factors for each PPFD and temperature combinations was calculated and averaged across all curves.

An Excel Spreadsheet-Based Tool for Evaluating Mesophyll Impact on Predicting Photosynthesis.

Purpose. Tool for Evaluating Mesophyll Impact on Predicting Photosynthesis (TEMIPP) is a Microsoft Excel spreadsheet-based, leaf-scale photosynthetic modeling tool. It is used for demonstrating the impact of lacking an explicit representation of mesophyll diffusion in a photosynthetic model on the predicted response of photosynthesis to the increase in atmospheric CO_2 concentrations.

Approach. TEMIPP simulates the measurement, analysis and application of curves of photosynthesis A against intercellular CO_2 concentrations C_i (i.e., the so-called A/C_i curves). A/C_i curves are typically measured at a saturating level of photosynthetic photon flux density (PPFD) and a fixed temperature. TEMIPP generates an A/C_i curve at a set of measuring environmental conditions (PPFD, temperature, atmospheric pressure, and oxygen) and a set of actual fundamental photosynthetic parameters (e.g., V_{cmax}, J_{max}, TPU, dark respiration R_d, mesophyll conductance g_m), all specified by the user. The photosynthetic rate is then calculated by applying the Farquhar–von Caemmerer–Berry (FvCB) model (46) extended with a finite g_m (36, 38). A g_m-lacking model, which is the FvCB model applied with an assumption of an infinite g_m, is fit to the generated A/C_i curve. The obtained key photosynthetic parameters are then used in the g_m-lacking model as in current carbon cycle models to predict photosynthesis at a new set of conditions that is different from the original set of measuring conditions under which the A/C_i curve for fitting was produced.

Instead of using simulated A/C_i curves, users have the option to apply real A/C_i measurements to TEMIPP. When real A/C_i curves are used, users will need to provide TEMIPP independently estimated photosynthetic parameters including g_m. Users can examine the impact of lacking an explicit representation of g_m by comparing model performance between the fitting to the original A/C_i curve and the prediction at new conditions. It is useful to check the residuals between the actual value and the value calculated by the g_m-lacking model as the residuals can reveal model performance more clearly than a simple direct comparison which can be misleading. Also it is important to compare the limitation states determined by the g_m-lacking model with the actual limitation states. This comparison will provide insight as to why an apparently well-calibrated g_m-lacking model can perform poorly in predictions.

The fitting uses the evolutionary method in Solver provided by Microsoft Excel. The Evolutionary algorithm is selected because the FvCB model is a classic change-point model, and its optimization is not smooth (38). If users do not wish to use the Microsoft Solver, they can use any optimization software they might have or LeafWeb (leafweb.ornl.gov) to estimate the parameters and then input their own parameters directly into TEMIPP.

The temperature response functions used in TEMIPP are from Sharkey et al. (41). If users wish to use different temperature response functions, they can input their own temperature response funcitons as well.

Detailed instructions.

i) Generate a new A/C_i curve. A new A/C_i curve can be generated in any of the following ways:

- *a*) Change the values of the standardized fundamental parameters Vcmax25, Jmax25, TPU25, gm25, Rd25 (cells E10–I10). Users can also change the Rubisco kinetic parameters (J10–L10) or the leaf absorptance parameter (M10) if they wish.
- *b*) Change the A/C_i curve measuring conditions of temperature, PPFD, atmospheric barometric pressure, and oxygen partial pressure (E20–H20).
- *c*) If they wish, users can provide their own coefficients in the temperature response functions in the section from E15 to L17.
- *d*) The A/C_i data for fitting are automatically computed from cells B36 to B53, depending on the values of C_i from A36 to A53. Users can adjust the C_i values from A36 to A53 as they wish. Leave any unused cell blank.

ii) Fit the g_m-lacking model:

- *a*) Click the cursor at Data in the top of Excel Spreadsheet.
- *b*) Click Solver. You may have to install the Excel Solver first.
- *c*) This brings up the Solver Parameters menu.
- *d*) The settings should have been already specified.
- *e*) Click Solve to minimize the value in the objective cell F54.
- *f*) Wait for the Solver to complete its job. This may take a while.

g) When Solver results menu appears, choose "Keep Solver Solution" and click OK.

iii) Provide a new set of environmental conditions for which the g_m-lacking model will make predictions. Put these values in E21–H21. Try different conditions to see how the performance of the g_m-lacking model vary as the conditions for prediction deviate from the conditions for which the original A/Ci curve for fitting was produced.

iv) Examine the two plots around row 70. Also check to see if the g_m-lacking model has identified the limitation states correctly (the limitation states are displayed in the section AD34–AE56 and AU34–AV136).

v) The default setting in the Solver Parameters menu is for optimizing Vcmax25, Jmax25, and Rd25 for the g_m-lacking model. TPU25 for the g_m-lacking model is set to be equal to that users provide in cell G10 to take advantage of the fact that TPU-limited photosynthesis is 3*TPU – R_d, which does not depend on CO_2 concentrations and therefore g_m. This avoids potential overfitting and unreasonable parameter values. However, if users wish to estimate TPU25 for the g_m-lacking model as well, go to the Solver Parameters menu, add ",G11" (without the quotation marks) after "I11" in the box under "By Changing Variable Cells."

vi) If they wish, users can also optimize for the Rubisco kinetic parameters for the g_m-lacking model by adding ",J11,K11,L11" under "By Changing Variable Cells" in the Solver Parameters menu. However, A/C_i data generally do not contain enough information to constrain all these parameters.

vii) Use real A/C_i measurements with independently estimated parameters. To use real A/C_i measurements with parameters estimated by other means for TEMIPP, do the following steps:

a) Save a copy of TEMIPP.
b) Manually input the real A/C_i data in the section A36–B53 and leave any unused cells blank (do not cut and paste as this will cause disabling of the auto-computing functions).
c) Input the standardized fundamental parameters estimated with explicit consideration of g_m into E10–L10 (TEMIPP can be modified to estimate g_m for the purpose of testing).
d) Input the A/C_i measuring conditions in E20–H20.
e) If in their A/C_i curve analysis, users used a set of coefficients for the temperature response functions different from those listed in TEMIPP, input the users' coefficients into the section E15–L17.
f) If users have independent estimates of the corresponding parameters for the g_m-lacking model, input them to E11–I11 and skip the Microsoft Solver; otherwise, invoke the Solver.
g) Check the plots and limitation states.

viii) Modify TEMIPP to estimate g_m and associated fundamental photosynthetic parameters.

a) Save a copy of TEMIPP.
b) Manually input the real C_i data in the section A36–A53 and leave any unused cells empty (do not cut and paste).
c) Manually input the A (net photosynthesis) data in the section M36–M53 and leave any unused cells empty (do not cut and paste).
d) If users wish to use a different set of coefficients for the temperature response functions, input these different coefficients into the section E15–L17.
e) Bring up the Solver.
f) Replace the content in "Set Objective:" with "O54" (without the quotation marks).
g) Replace the content in "By Changing Variable Cells:" with "E10,F10,G10,H10,I10".
h) Replace all "$11"s in the box under "Subject to the Constraints" with "$10".
i) Click Solve.
j) Wait for the Solver to complete its job.
k) The optimized parameters will be displayed in the cells from E10–I10.

TEMIPP is meant to be a demonstration tool only. For actual A/C_i curve analyses, methods such as LeafWeb (leafweb.ornl.gov) are more appropriate (38).

1. Warren CR (2008) Stand aside stomata, another actor deserves centre stage: The forgotten role of the internal conductance to CO_2 transfer. *J Exp Bot* 59(7):1475–1487.
2. Niinemets U, Díaz-Espejo A, Flexas J, Galmés J, Warren CR (2009a) Role of mesophyll diffusion conductance in constraining potential photosynthetic productivity in the field. *J Exp Bot* 60(8):2249–2270.
3. Nobel PS (1977) Internal leaf area and cellular CO_2 resistance: Photosynthetic implications of variations with growth conditions and plant species. *Physiol Plant* 40(2): 137–144.
4. Flexas J, Ribas-Carbó M, Diaz-Espejo A, Galmés J, Medrano H (2008) Mesophyll conductance to CO_2: Current knowledge and future prospects. *Plant Cell Environ* 31(5): 602–621.
5. Bernacchi CJ, Portis AR, Nakano H, von Caemmerer S, Long SP (2002) Temperature response of mesophyll conductance. Implications for the determination of Rubisco enzyme kinetics and for limitations to photosynthesis in vivo. *Plant Physiol* 130(4): 1992–1998.
6. Chazen O, Neumann PM (1994) Hydraulic signals from the roots and rapid cell-wall hardening in growing maize (Zea mays L.) leaves are primary responses to polyethylene glycol-induced water deficits. *Plant Physiol* 104(4):1385–1392.
7. Miyazawa SI, Yoshimura S, Shinzaki Y, Maeshima M, Miyake C (2008) Deactivation of aquaporins decreases internal conductance to CO_2 diffusion in tobacco leaves grown under long-term drought. *Funct Plant Biol* 35(7):553–564.
8. Kaldenhoff R (2012) Mechanisms underlying CO_2 diffusion in leaves. *Curr Opin Plant Biol* 15(3):276–281.
9. Gu L, Sun Y (2014) Artefactual responses of mesophyll conductance to CO2 and irradiance estimated with the variable J and online isotope discrimination methods. *Plant Cell Environ* 37(5):1231–1249.
10. Tholen D, Ethier G, Genty B, Pepin S, Zhu XG (2012) Variable mesophyll conductance revisited: Theoretical background and experimental implications. *Plant Cell Environ* 35(12):2087–2103.
11. Nobel PS (2009) *Physicochemical and Environmental Plant Physiology* (Academic Press, Oxford, UK), 4th Ed.
12. Cernusak LA, et al. (2013) Environmental and physiological determinants of carbon isotope discrimination in terrestrial plants. *New Phytol* 200(4):950–965.
13. Sun Y, et al. (2014) Asymmetrical effects of mesophyll conductance on fundamental photosynthetic parameters and their relationships estimated from leaf gas exchange measurements. *Plant Cell Environ* 37(4):978–994.
14. Niinemets U, Wright IJ, Evans JR (2009c) Leaf mesophyll diffusion conductance in 35 Australian sclerophylls covering a broad range of foliage structural and physiological variation. *J Exp Bot* 60(8):2433–2449.
15. Niinemets U (2007) Photosynthesis and resource distribution through plant canopies. *Plant Cell Environ* 30(9):1052–1071.
16. Terashima I, Hanba YT, Tazoe Y, Vyas P, Yano S (2006) Irradiance and phenotype: Comparative eco-development of sun and shade leaves in relation to photosynthetic CO_2 diffusion. *J Exp Bot* 57(2):343–354.
17. Hanba YT, Kogami H, Terashima I (2002) The effect of growth irradiance on leaf anatomy and photosynthesis in Acer species differing in light demand. *Plant Cell Environ* 25(8):1021–1030.
18. Piel C, Frak E, Le Roux X, Genty B (2002) Effect of local irradiance on $CO(_2)$ transfer conductance of mesophyll in walnut. *J Exp Bot* 53(379):2423–2430.
19. Laisk A, et al. (2005) Adjustment of leaf photosynthesis to shade in a natural canopy: Rate parameters. *Plant Cell Environ* 28(3):375–388.
20. Warren CR, Low M, Matyssek R, Tausz M (2007) Internal conductance to CO_2 transfer of adult Fagus sylvatica: Variation between sun and shade leaves and due to free-air ozone fumigation. *Environ Exp Bot* 59(2):130–138.
21. Montpied P, Granier A, Dreyer E (2009) Seasonal time-course of gradients of photosynthetic capacity and mesophyll conductance to CO_2 across a beech (Fagus sylvatica L.) canopy. *J Exp Bot* 60(8):2407–2418.
22. Han Q, Iio A, Naramoto M, Kakubari Y (2010) Response of internal conductance to soil drought in sun and shade leaves of adult. *Acta Silv. Lign. Hung.* 6:123–134.
23. Campbell GS, Norman JM (1998) *An Introduction to Environmental Biophysics* (Springer, New York).
24. Richardson JJ, Kim SH, Moskal LM (2009) Modeling approaches to estimate effective leaf area index from aerial discrete-return LIDAR. *Agric For Meteorol* 149(6-7):1152–1160.
25. Warren CR, Dreyer E (2006) Temperature response of photosynthesis and internal conductance to CO_2: Results from two independent approaches. *J Exp Bot* 57(12): 3057–3067.

26. Yamori W, Noguchi K, Hanba YT, Terashima I (2006) Effects of internal conductance on the temperature dependence of the photosynthetic rate in spinach leaves from contrasting growth temperatures. *Plant Cell Physiol* 47(8):1069–1080.
27. Scafaro AP, Von Caemmerer S, Evans JR, Atwell BJ (2011) Temperature response of mesophyll conductance in cultivated and wild Oryza species with contrasting mesophyll cell wall thickness. *Plant Cell Environ* 34(11):1999–2008.
28. Evans JR, von Caemmerer S (2013) Temperature response of carbon isotope discrimination and mesophyll conductance in tobacco. *Plant Cell Environ* 36(4):745–756.
29. Keenan T, Sabate S, Gracia C (2010a) The importance of mesophyll conductance in regulating forest ecosystem productivity during drought periods. *Glob Change Biol* 16(3):1019–1034.
30. Keenan T, Sabate S, Gracia C (2010b) Soil water stress and coupled photosynthesis-conductance models: Bridging the gap between conflicting reports on the relative roles of stomatal, mesophyll conductance and biochemical limitations to photosynthesis. *Agric For Meteorol* 150(3):443–453.
31. Egea G, Verhoef A, Vidale PL (2011) Towards an improved and more flexible representation of water stress in coupled photosynthesis-stomatal conductance models. *Agric For Meteorol* 151(10):1370–1384.
32. Oliver RJ, Taylor G, Finch JW (2012) Assessing the impact of internal conductance to CO2 in a land-surface scheme:Measurement and modelling of photosynthesis in Populus nigra. *Agric For Meteorol* 152:240–251.
33. Oleson KW, et al. (2013) Technical description of version 4.5 of the community land model (CLM). *NCAR Technical Note.* www.cesm.ucar.edu/models/cesm1.2/clm/. Accessed October 2, 2013.
34. Bonan GB, et al. (2011) Improving canopy processes in the Community Land Model version 4 (CLM4) using global flux fields empirically inferred from FLUXNET data. *J Geophys Res* 116(G2):G02014.
35. Niinemets U, Díaz-Espejo A, Flexas J, Galmés J, Warren CR (2009b) Importance of mesophyll diffusion conductance in estimation of plant photosynthesis in the field. *J Exp Bot* 60(8):2271–2282.
36. Ethier GJ, Livingston NJ (2004) On the need to incorporate sensitivity to CO_2 transfer conductance into the Farquhar-von Caemmerer-Berry leaf photosynthesis model. *Plant Cell Environ* 27(2):137–153.
37. Zeng W, Zhou GS, Jia BR, Jiang YL, Wang Y (2010) Comparison of parameters estimated from A/C_i and A/C_c curve analysis. *Photosynthetica* 48(3):323–331.
38. Gu L, Pallardy SG, Tu K, Law BE, Wullschleger SD (2010) Reliable estimation of biochemical parameters from C_3 leaf photosynthesis-intercellular carbon dioxide response curves. *Plant Cell Environ* 33(11):1852–1874.
39. Collatz GJ, Ball JT, Grivet C, Berry JA (1991) Physiological and environmental regulation of stomatal conductance, photosynthesis and transpiration: A model that includes a laminar boundary layer. *Agric For Meteorol* 54(2-4):107–136.
40. Long SP, Bernacchi CJ (2003) Gas exchange measurements, what can they tell us about the underlying limitations to photosynthesis? Procedures and sources of error. *J Exp Bot* 54(392):2393–2401.
41. Sharkey TD, Bernacchi CJ, Farquhar GD, Singsaas EL (2007) Fitting photosynthetic carbon dioxide response curves for C_3 leaves. *Plant Cell Environ* 30(9):1035–1040.
42. Piao S, et al. (2013) Evaluation of terrestrial carbon cycle models for their response to climate variability and to CO_2 trends. *Glob Change Biol* 19(7):2117–2132.
43. Hurtt GC, et al. (2011) Harmonization of land-use scenarios for the period 1500-2100: 600 years of global gridded annual land-use transitions, wood harvest, and resulting secondary lands. *Clim Change* 109(1-2):117–161.
44. Beer C, et al. (2010) Terrestrial gross carbon dioxide uptake: Global distribution and covariation with climate. *Science* 329(5993):834–838.
45. Welp LR, et al. (2011) Interannual variability in the oxygen isotopes of atmospheric CO2 driven by El Niño. *Nature* 477(7366):579–582.
46. Farquhar GD, von Caemmerer S, Berry JA (1980) A biochemical model of photosynthetic CO_2 assimilation in leaves of C $_3$ species. *Planta* 149(1):78–90.

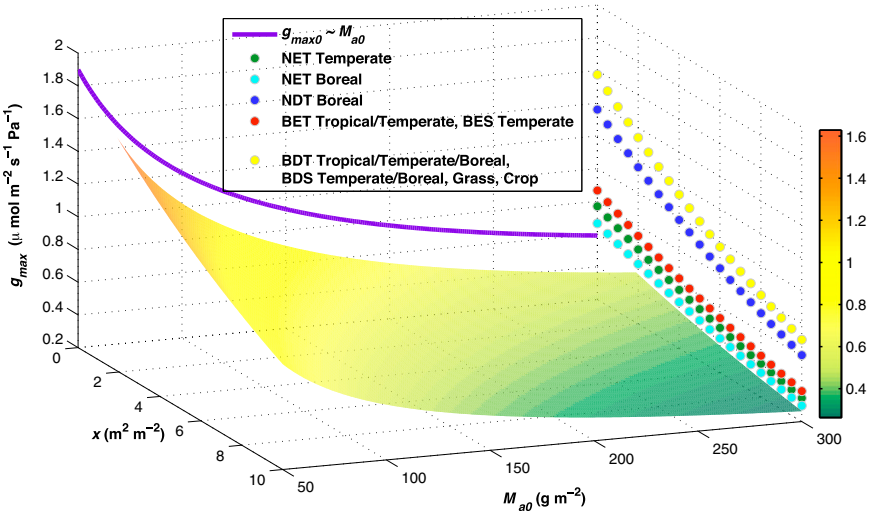

Fig. S1. The g_m model (scaled to the leaf temperature of 25 °C and saturating soil moisture). The 3D surface shows the maximum mesophyll conductance g_{max} [$=a \cdot M_{a0}^{b} \cdot \exp(-k_g \cdot x)$, the product of Eqs. **S2** and **S7**] as a function of canopy-top M_a (M_{a0}) and cumulative leaf area index (x). The purple curve in the $x = 0$ plane shows the relationship between g_{max0} and M_{a0} (Eq. **S2**). The dotted curves show the g_m profile within canopy (Eq. **S7**) for the specified PFTs in CLM4.5. The values of M_{a0} are PFT specific, calculated from the canopy top-specific leaf area SLA_0 in CLM4.5. For clarity, we display these dotted curves on the $M_{a0} = 300$ (g/m^2) plane. Here, NET, NDT, BET, BDT, and BDS denote needleleaf evergreen tree, needleleaf deciduous tree, broadleaf evergreen tree, broadleaf deciduous tree, and broadleaf deciduous shrub, respectively.

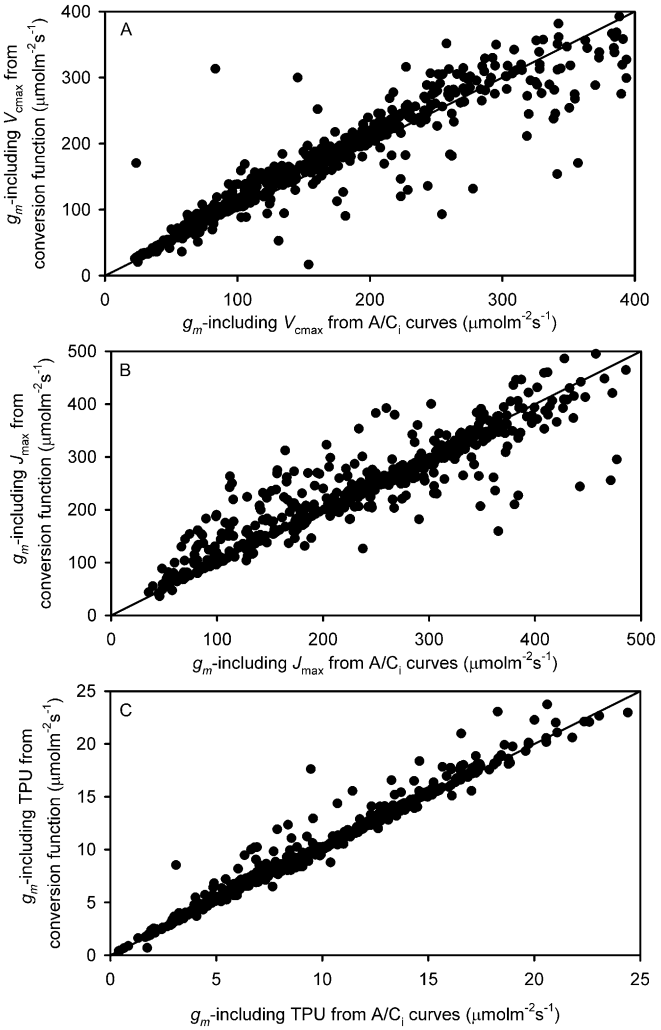

Fig. S2. Comparison of the g_m-including (*A*) V_{cmax}, (*B*) J_{max}, and (*C*) TPU predicted with the colimiting conversion function to corresponding values optimized directly from A/C_i curves with the colimiting FvCB model. In each plot, the 1:1 line is included as a reference. The correlation coefficient is 0.91, 0.87, and 0.98 for V_{cmax}, J_{max}, and TPU, respectively.

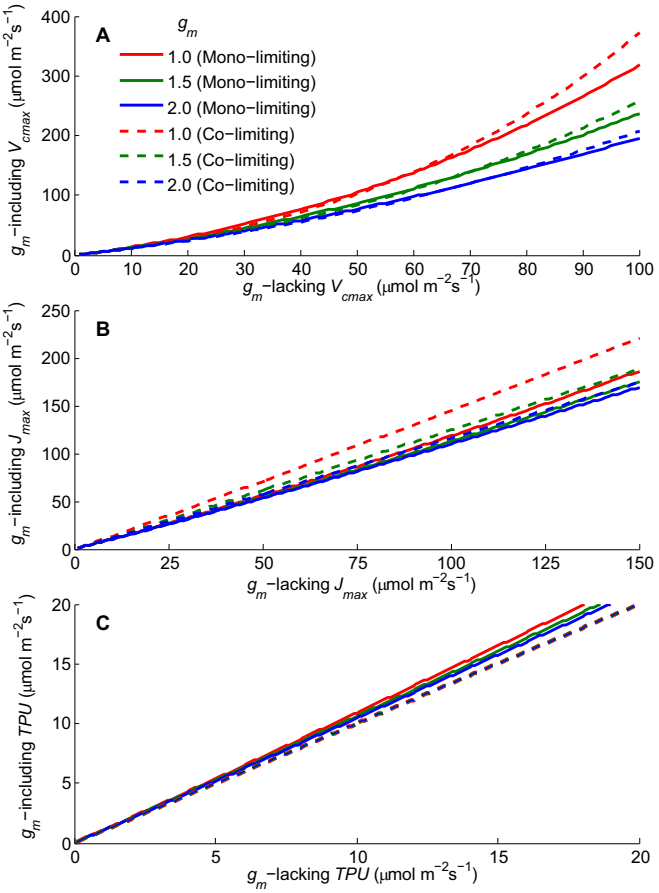

Fig. S3. The comparison of the monolimiting (solid curves) and colimiting (dashed curves) conversion functions at different values of mesophyll conductance g_m (μmol/m^2/s/Pa) for (*A*) V_{cmax}, (*B*) J_{max}, and (*C*) TPU.

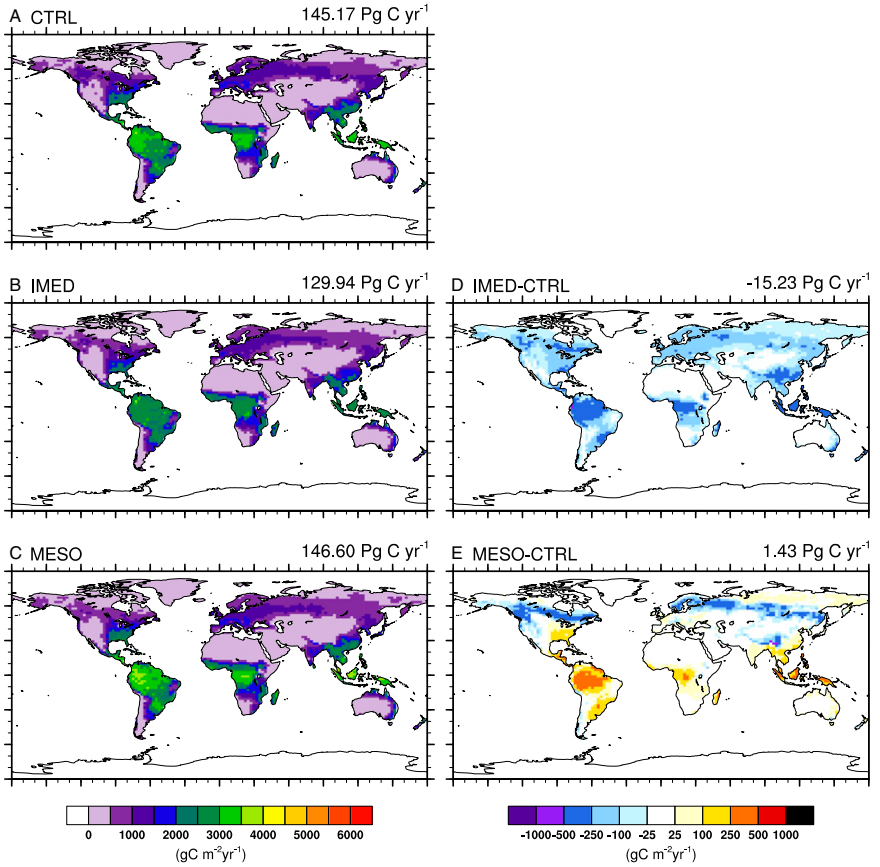

Fig. S4. Mean annual GPP (gC/m^2/y) of the period 1985–2004 for the simulation of (*A*) CTRL, the control simulation with CLM4.5; (*B*) IMED, the intermediate simulation with mesophyll conductance model and g_m-lacking photosynthetic parameters; and (*C*) MESO, the final, fully updated simulation with mesophyll conductance model and g_m-including photosynthetic parameters. (*D* and *E*) Differences from the CTRL simulation for the IMED and MESO simulations, respectively. The value shown on the *Upper Right* of each panel is the estimated mean annual global GPP (PgC/y). All simulations are driven by reanalysis climate and observed atmospheric CO_2 concentrations. The colimiting conversion function is used in these simulations.

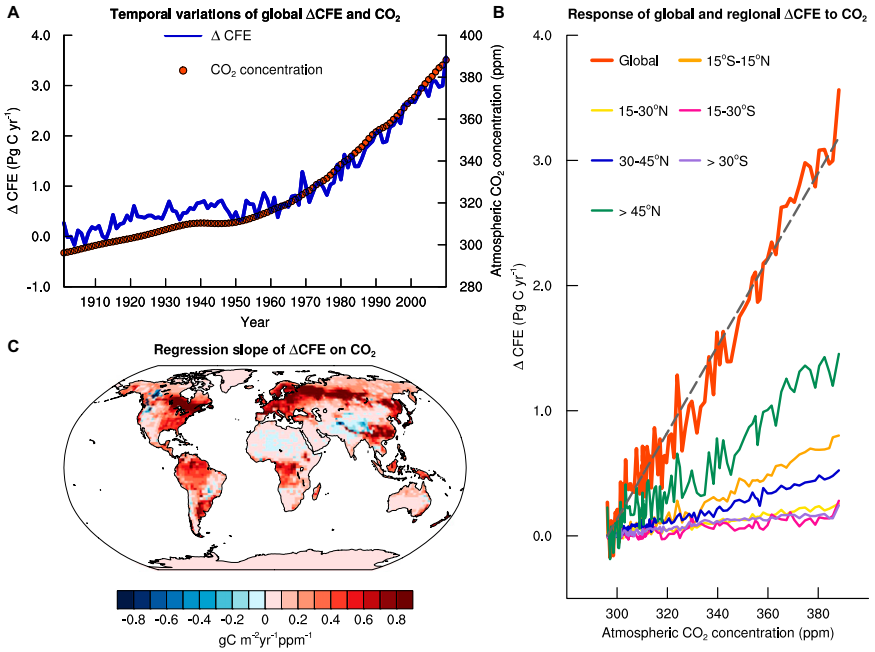

Fig. S5. Temporal and spatial variations of the difference in the CO_2 fertilization effect (ΔCFE, PgC/y) on annual gross primary production simulated with CLM4.5 between with and without explicit consideration of mesophyll conductance (g_m). The monolimiting conversion function is used to establish the g_m-lacking to g_m-including photosynthetic parameter correspondence. (*A*) Historical trends in ΔCFE (blue curve, left ordinate) and in atmospheric CO_2 concentration (ppm, red dots, right ordinate) from 1901 to 2010. (*B*) The variation of the global and latitudinal ΔCFE with atmospheric CO_2 concentration. The global curve (red) is fitted with a line ($y = -10.233 + 0.035x$, $r^2 = 0.96$). (*C*) The global variation in the slope (gC/m^2/y/ppm) of the linear regression of the grid-based ΔCFE as a function of atmospheric CO_2 concentration.

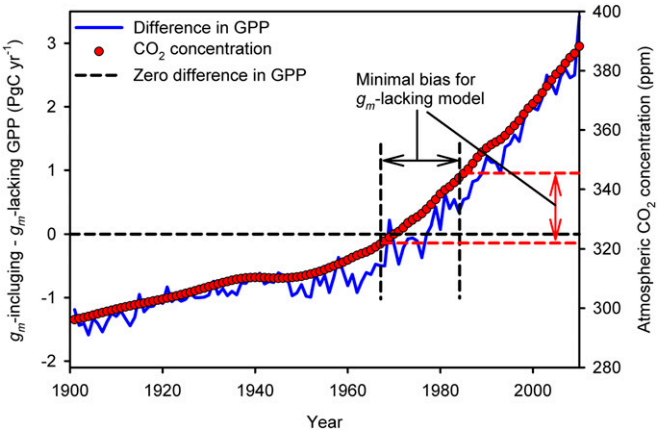

Fig. S6. Temporal variation of the difference in the annual global GPP simulated with CLM4.5 between with and without explicit consideration of mesophyll conductance (g_m). This figure is similar to Fig. 1*A* except that there is no offset in the baseline reference GPP between the two models. The colimiting conversion function is used to establish the g_m-lacking to g_m-including photosynthetic parameter correspondence. The historical atmospheric CO_2 concentration is also shown. The two dash vertical (black) and horizontal (red) lines identify the years and the range of atmospheric CO_2, respectively, in which the g_m-lacking model has minimal bias.

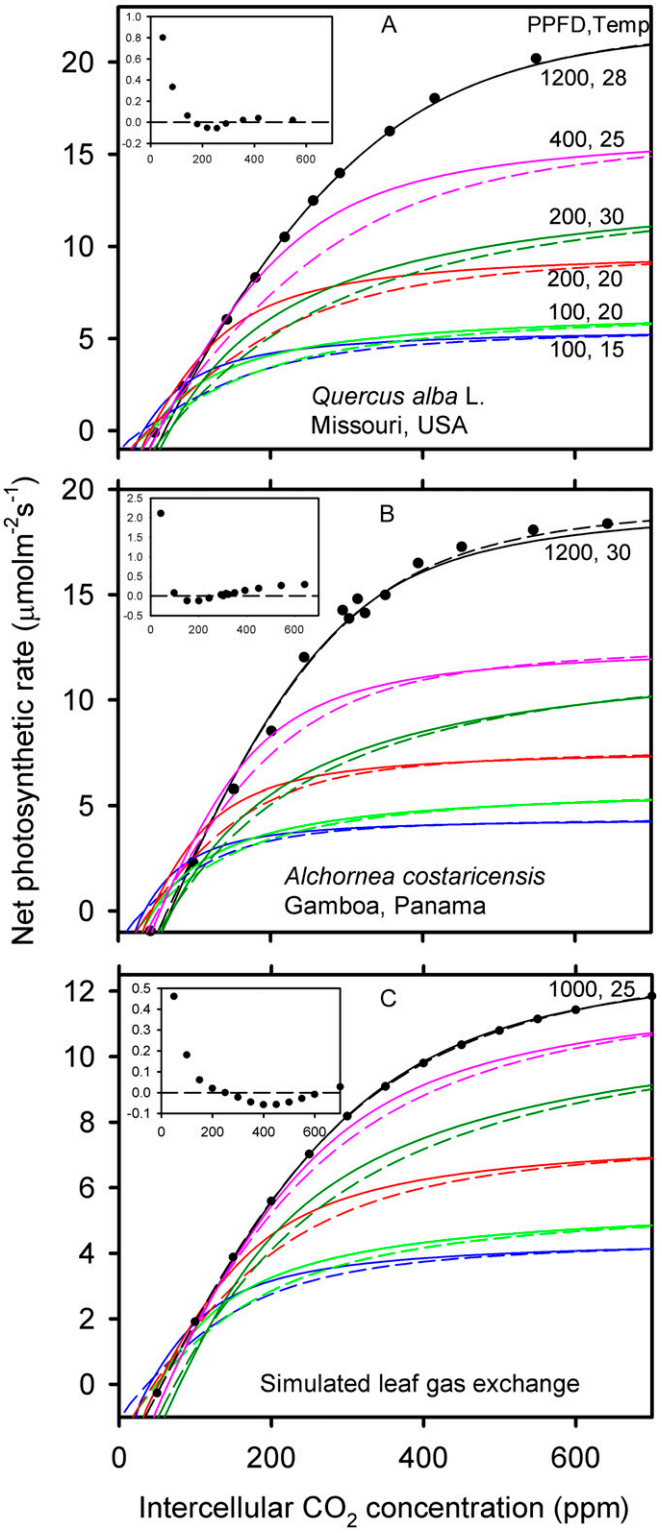

Fig. S7. Typical examples of the contrast in leaf net photosynthetic rate as a function of intercellular CO_2 concentration calculated with a leaf photosynthetic model between including (dashed curves) and lacking (solid curves) explicit consideration of mesophyll conductance (g_m). In each panel, the uppermost dashed and solid curves represent direct fitting of the g_m-including and g_m-lacking models, respectively, to the data (dots) measured (*A* and *B*) or simulated (*C*) at indicated PPFD (μmol/m^2/s) and temperatures (°C). The difference in fit between the g_m-including and g_m-lacking models is more clearly seen in the *Inset* of each panel, which shows the difference in calculated leaf photosynthetic rate (*y* axis, μmol/m^2/s) as a function of intercellular CO_2 concentration (ppm). The photosynthetic parameters obtained in the fittings are then used to calculate photosynthesis at other PPFD and temperatures, which are indicated in *A* only but are the same in *B* and *C*.

Table S1. Empirical constants used in the g_m model

Symbol	Equation	Value	Source
Modeling mesophyll conductance at canopy top			
a	Eq. **S2**	24.240338	Fit from Niinemets et al. (2)
b		−0.6509	
Canopy integration of mesophyll conductance			
d	Eqs. **S3, S4, S7**	0.8109	Fit from Montpied et al. (21)
f	Eqs. **S5, S7**	0.221897	Fit from Niinemets (15)
k_l	Eqs. **S6, S7**	0.5	Theoretical value (23)
k_g	Eq. **S7**	0.08997	$=k_l \cdot d \cdot f$
Temperature response function			
c	Eq. **S8**	20	Bernacchi et al. (5)
ΔH_a		49.6×10^3 J/mol	
ΔH_d		437.4×10^3 J/mol	
ΔS		1.4×10^3 J/mol/K	

Table S2. Empirical constants in the conversion function that relates the g_m-lacking to g_m-including parameters at a reference temperature of 25 °C

Photosynthetic parameter (μmol/m^2/s)	p	q	u	v	r^2	RMS (μmol/m^2/s)	Source
Monolimiting conversion function							
V_{cmax}	0.1164	1.2643	0.6429	0.9431	0.83	18.0437	Sun et al. (13)
J_{max}	0.0084	0.7552	0.6230	−0.1166	0.97	7.5290	
TPU	0.1249	1.8059	0.2525	1.5905	0.99	0.3597	
Colimiting conversion function							
V_{cmax}	0.0340	1.1253	0.8787	0.4801	0.83	42.9184	This study
J_{max}	0.2935	1.4838	0.0858	0.1726	0.75	62.7638	
TPU	0	0	0	0	0.97	0.9254	

Two sets of constants are given: one is for the monolimiting FvCB model and reproduced from Sun et al. (13) and the other is for the colimiting FvCB model and estimated in this study. TPU for the colimiting FvCB model differs little between the g_m-including and -lacking considerations and as such all its associated constants are effectively zero (Eq. **S14**).

Table S3. Values of key photosynthetic parameters for each PFT in CLM4.5

PFTs	M_{a0} (gC/m^2)*	g_{max0} (μmol/m^2/s/Pa)	g_m-lacking V_{cmax} (μmol/m^2/s)	g_m-lacking J_{max} (μmol/m^2/s)	g_m-including V_{cmax} (μmol/m^2/s)†	g_m-including J_{max} (μmol/m^2/s)
NET temperate	100.00	1.21	62.50	107.19	132.16 (132.31)	143.59 (124.39)
NET boreal	125.00	1.05	62.60	107.36	145.20 (143.68)	152.81 (127.06)
NDT boreal	41.67	2.14	39.10	67.06	52.83 (55.23)	76.29 (71.89)
BET tropical	83.33	1.36	55.00	94.33	100.90 (103.48)	120.77 (106.83)
BET temperate	83.33	1.36	61.50	105.47	120.11 (121.29)	135.36 (120.53)
BDT tropical	33.33	2.47	41.00	70.32	53.89 (55.91)	78.14 (74.94)
BDT temperate	33.33	2.47	57.70	98.96	83.47 (84.91)	110.32 (107.07)
BDT boreal	33.33	2.47	57.70	98.96	83.47 (84.91)	110.32 (107.07)
BES temperate	83.33	1.36	61.70	105.82	120.73 (121.85)	135.81 (120.96)
BDS temperate	33.33	2.47	54.00	92.61	76.50 (78.20)	103.18 (99.89)
BDS boreal	33.33	2.47	54.00	92.61	76.50 (78.20)	103.18 (99.89)
C3 arctic grass	33.33	2.47	78.20	134.11	126.66 (125.09)	149.94 (147.52)
C3 grass	33.33	2.47	78.20	134.11	126.66 (125.09)	149.94 (147.52)

Leaf temperature and mean growth temperature are assumed to be 25 °C. Here the mean growth temperature refers to the 10-d mean air temperature, which is used to account for the acclimation effect of J_{max}/V_{cmax} ratio in CLM (33). BDS, broadleaf deciduous shrub; BDT, broadleaf deciduous tree; BES, broadleaf evergreen shrub; BET, broadleaf evergreen tree; NDT, needleleaf deciduous tree; NET, needleleaf evergreen tree.

*Some PFTs share the same values of SLA_0 and therefore M_{a0} (=$1/SLA_0$) in CLM, which leads to the same values of M_a and g_{max} at canopy top for these PFTs.

†Two sets of V_{cmax} and J_{max} values are shown here when g_m is included, corresponding to colimiting and monolimiting conversion functions, respectively. Values in parentheses are those from the application of the monolimiting conversion function.

Table S4. Summary of global simulations

Simulation	Description
Transient CO_2 simulations	
CTRL	Control simulations with the default CLM4.5
IMED	Intermediate simulations that use CLM4.5 with the mesophyll conductance (g_m) model only, but retain the original phenomenological (g_m-lacking) photosynthetic parameters
MESO	Fully updated simulations that use CLM4.5 with the g_m model and the g_m-including photosynthetic parameters
Constant CO_2 simulations	
CTRL_cCO_2	Same as CTRL, but with a constant atmospheric CO_2 concentration (296 ppm at 1901)
MESO_cCO_2	Same as MESO, but with a constant atmospheric CO_2 concentration (296 ppm at 1901)

The MESO simulations are repeated with the colimiting and monolimiting conversion functions.

Other Supporting Information Files

Dataset S1 (XLSX)